ACS APPLIED BIO MATERIALS

www.acsabm.org

Article

Virus-Free Method to Control and Enhance Extracellular Vesicle Cargo Loading and Delivery

Sheryl Bui, Julia Dancourt, and Gregory Lavieu*

Cite This: *ACS Appl. Bio Mater.* 2023, 6, 1081−1091

Read Online

ACCESS | Metrics & More | Article Recommendations | Supporting Information

ABSTRACT: Extracellular vesicles (EVs)—including exosomes and microvesicles—are involved in cell−cell communication. EVs encapsulate different types of molecules such as proteins or nucleotides and are long-lasting contenders for the establishment of personalized drug delivery systems. Recent studies suggest that the intrinsic capacities for uptake and cargo delivery of basic EVs might be too limited to serve as a potent delivery system. Here, we develop two synergistic methods to, respectively, control EV cargo loading and enhance EV cargo delivery through fusion without requirement for any viral fusogenic protein. Briefly, cargo loading is enabled through a reversible drug-inducible system that triggers the interaction between a cargo of interest and CD63, a well-established transmembrane EV marker. Enhanced cargo delivery is promoted by overexpressing Syncytin-1, an endogenous retrovirus envelop protein with fusogenic properties encoded by the human genome. We validate our bioengineered EVs in a qualitative and quantitative manner. Finally, we utilize this method to develop highly potent killer EVs, which contain a lethal toxin responsible for protein translation arrest and acceptor cell death. These advanced methods and future downstream applications may open promising doors in the manufacture of virus-free and EV-based delivery systems.

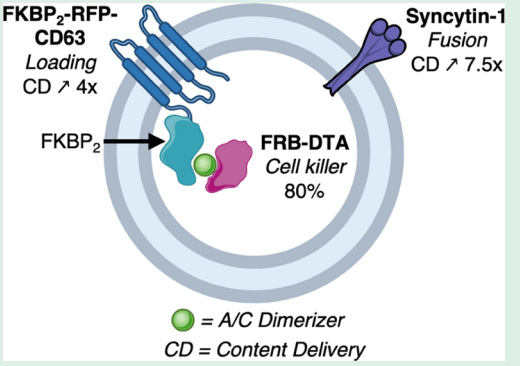

KEYWORDS: *extracellular vesicles, drug delivery system, uptake, content delivery, EV loading, Syncytin-1, killer EV*

INTRODUCTION

Extracellular vesicles (EVs) are physiological vectors of cell−cell communication. They include microvesicles and exosomes, which are, respectively, secreted directly from the plasma membrane or released from multivesicular bodies—an endosomal compartment.[1] EVs are involved in many physiological functions and diseases and can carry several types of cargoes, including proteins, nucleotides, lipids,[1] or synthetic drugs.[2] EVs can cross biological barriers such as the blood−brain barrier[3] and have a higher biocompatibility than liposomes.[4] All of these properties make EVs excellent candidates for a new generation of drug delivery systems (DDS).

Importantly, the molecular mechanisms underlying EV uptake and content delivery within the acceptor cell cytosol are still poorly characterized.[1,5] Several studies,[6−8] including ours, established that EV cargo delivery within acceptor cells occurs with a limited efficiency at the basal level. This suggests that the basic properties of EVs must be modified to act as potent delivery vectors.

At least two steps of the delivery process can be manipulated to potentiate the release of an EV cargo within acceptor cells.[4,9] One is the loading of the cargo into EVs and the second is the fusion between the EV membrane and the target membrane that enables EV cargo delivery.

EV cargo loading can be exogenous (per- or post-EV isolation) or endogenous through the manipulation of donor cells (preisolation).[4,10] Exogenous loading occurs after or during EV production by chemical or physical methods. These methods are highly useful for synthetic molecules but risk to impair the EV membrane and inner composition. The endogenous loading of protein cargo into EVs can be enabled through the use of lipidation motifs such as myristoylation and palmitoylation signals[11] fused to an overexpressed protein of interest. More recently, drug-inducible and reversible systems have been used to load protein cargoes with variable efficiencies.[11−14]

Concerning the fusion step, the glycoprotein envelope of the vesicular stomatitis virus (VSV-G) is the gold standard in the DDS field.[15] Briefly, VSV-G mediates membrane fusion after being activated by endosomal acidification.[16,17] This protein is highly efficient, but its viral origin conveys a risk of immunogenicity related to a massive humoral response,[15,18] which prevent multidose therapies. So far, at least two strategies were proposed to solve this problem in other fields: to hide the full VSV with carrier cells,[19] which is incompatible

Received: November 17, 2022
Accepted: January 28, 2023
Published: February 13, 2023

https://doi.org/10.1021/acsabm.2c00955
ACS Appl. Bio Mater. 2023, 6, 1081−1091

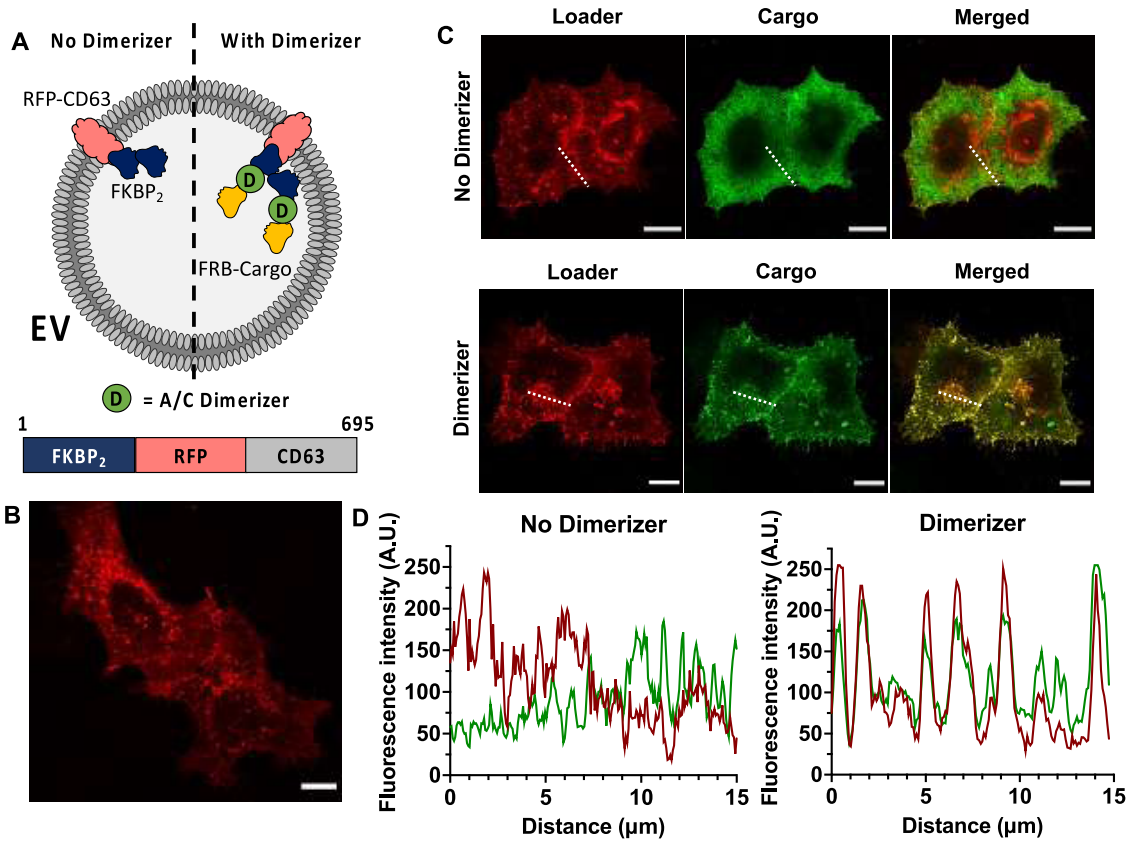

Figure 1. EV loading system proof of concept. (A) RFP-CD63 was fused in the N-terminal with two FKBP domains able to dimerize with FRB domains in the presence of a rapamycin-like dimerizer drug (A/C dimerizer, Takara Bio.). The FRB domain can be fused to any cargo of interest. (B) Confocal imaging of $FKBP_2$-RFP-CD63 (loader) transiently expressed in wild-type HeLa cells. Representative of three independent experiments. Scale bar, 10 μm. (C) A recruitment assay was performed by incubating (dimerizer) or not (no dimerizer) HeLa cells expressing loader (red) and cargo (FRB-NLuc-HA; green) with the A/C dimerizer. Cells were imaged by confocal microscopy. Merged images show the presence of colocalization in yellow. Representative of two independent experiments. Scale bar, 10 μm. The fluorescence intensity of both loader (red) and cargo (green) was plotted along the white dotted line in panel (D). A.U., arbitrary unit.

with EV delivery, or to replace VSV-G with other viral glycoproteins,[18] which does not solve the viral immunogenicity issue. Also, these two propositions complexify the technology, hence increasing the safety steps toward therapeutic applications.

To address this issue, we propose the use of an alternative fusogen, Syncytin-1 (Syn1), an endogenous human protein derived from an ancestral retroviral envelop protein involved in placenta formation[20] and immunotolerance.[21] This protein is cleaved during its maturation, has two domains—transmembrane and extracellular—linked by a disulfide bond,[22] and mediates membrane fusion after binding its cognate receptor, the alanine serine cysteine transporter 2 (ASCT2), located at the plasma membrane.[23]

Although several studies reported novel methods to bioengineer EVs for future therapeutic applications,[4,9] no systematic quantification was made to precisely measure the benefits of the different methods, preventing rigorous analytical interstudy comparisons. This minimizes the impact of these studies and putative future use and integration in manufacturing processes. This situation calls for quantitative research on EV uptake and delivery and for standardization in the EV engineering field.[5,24]

Here, we use a cargo-based approach where we follow the fate of a luminescent cargo, the NanoLuciferase[6,25] (NLuc), to precisely measure the efficiency of our enhanced loading and/or fusion methods. The NLuc allows quantitative and qualitative measurement of EV cargo loading, EV uptake (which encompasses cell surface binding, internalization, and content delivery), and EV cargo delivery within acceptor cells.

Finally, we combine both enhanced loading and fusion methods to bioengineer killer EVs, decorated with Syn1 and containing a lethal toxin. We demonstrate that the toxin is efficiently loaded into EVs and then delivered within the acceptor cell where protein translation is arrested leading to cell death. The results presented here suggest that our approach may contribute to the development of efficient virus-free EV-based delivery systems.

RESULTS

Development of an EV Cargo Loading System. *EV Cargo Loading Characterization.* We took advantage of the well-established FRB/FKBP heterodimerization system,[26] in which FKBP (FK506 binding protein) and FRB (FKBP-rapamycin binding) domains are able to dimerize in the presence of a biologically innocuous rapamycin analog dimerizer drug, the A/C dimerizer.[27] This interaction is reversible, and the two domains can be easily fused to overexpressed proteins to induce their dimerization within the donor cells.

The cluster of differentiation 63 (CD63) is a tetraspanin found to be generally highly enriched in EV membranes.[28] We

https://doi.org/10.1021/acsabm.2c00955
ACS Appl. Bio Mater. 2023, 6, 1081−1091

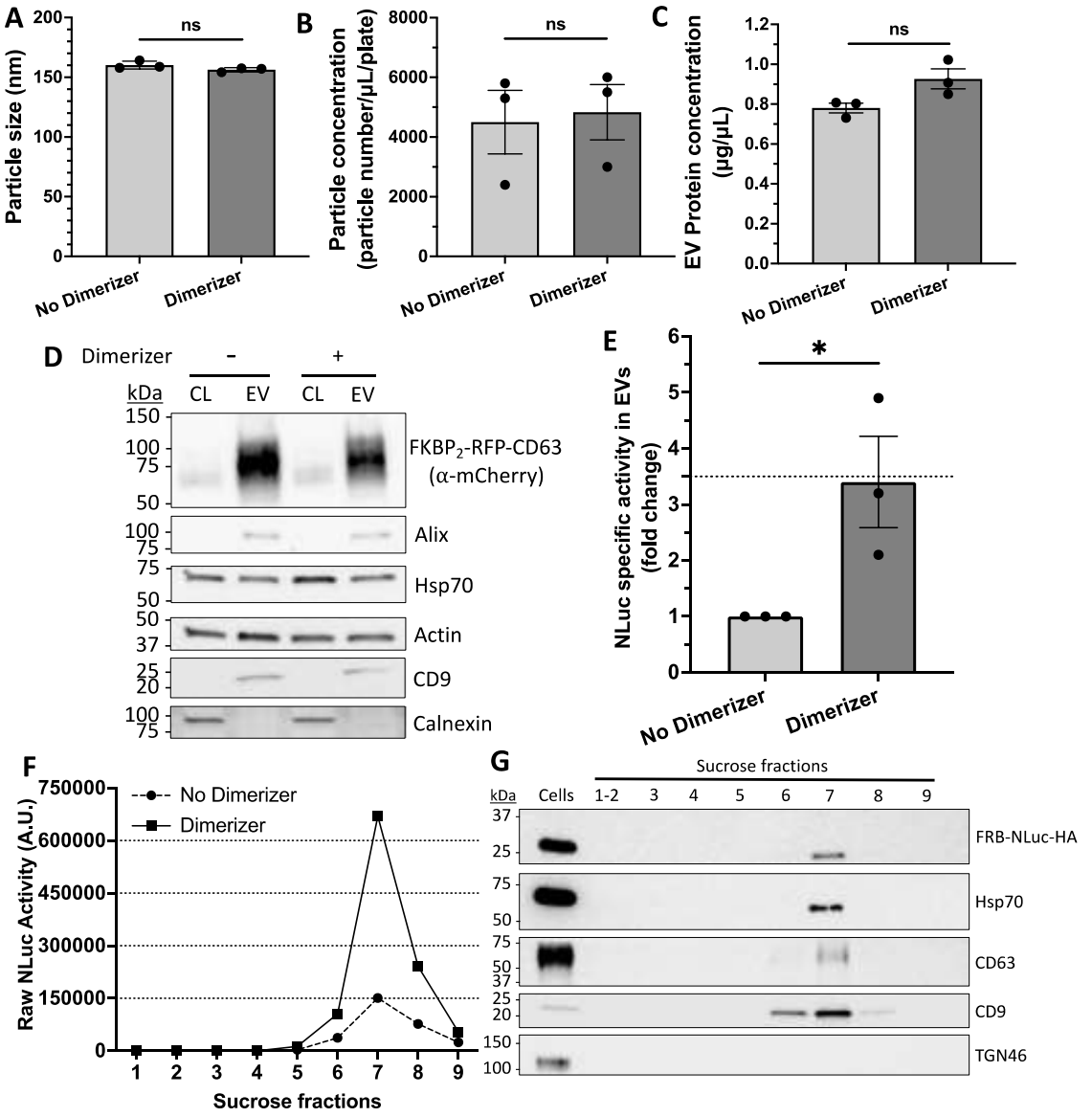

Figure 2. EV loading characterization. EVs were produced by cells as in Figure 1. (A) Particle size and (B) concentration were measured by nanoparticle tracking analysis and (C) EV protein concentration by BCA. (A−C) Each dot represents the mean of a technical duplicate. Mean ± SEM is represented. (D) Cell lysates (CLs) and EVs from cells treated ("+") or not ("−") with the A/C dimerizer drug were analyzed by Western blot with different markers: RFP (via α-mCherry antibody), ALIX, Hsp70, actin, CD9, and calnexin. Equal amounts of protein were loaded. Representative of two independent experiments. (E) FRB-NLuc-HA specific activity in the EVs was normalized on the "no dimerizer" condition and plotted. Each dot represents the mean of a technical duplicate. Mean ± SEM is represented. (F) A floatation assay was performed on "no dimerizer" and "dimerizer" EVs. The respective FRB-NLuc-HA activity of each fraction was plotted. A.U., arbitrary unit. (G) Fractions obtained after the floatation of the "dimerizer" condition were analyzed by Western blot to monitor the cargo (FRB-NLuc-HA), Hsp70, CD63, CD9, and TGN46. For statistical analysis, a Wilcoxon test was performed with $p \geq 0.05$ nonsignificant (ns) and $p < 0.05$ significant (*).

decided to append two FKBP domains to the N-terminus of CD63 tagged with the red fluorescent protein (RFP) and to coexpress it with FRB-tagged proteins of interest in the EV donor cells. In the presence of the dimerizer, we expect $FKBP_2$-RFP-CD63 to capture the FRB-tagged proteins in the EVs and thus to increase their EV loading. For the cargo of interest, we first fused FRB to NLuc-HA, which contained NanoLuciferase (NLuc) for highly sensitive luminescent detection[6,25] and HA tag for Western blot and immunofluorescence (Figure 1A).

$FKBP_2$-RFP-CD63 (hereafter named loader) was first transiently expressed in HeLa cells on its own, and confocal microscopy revealed that the chimeric protein localized mainly to endosomal compartments and to some extent to the plasma membrane, as expected (Figure 1B).[1,28] This result was also confirmed by other cell types: HEK293T, SW480 (colon adenocarcinoma), and EGI-1 (cholangiocarninoma) (Figure S1). This showed that the $FKBP_2$ domain did not alter the intracellular localization of the chimeric CD63.

We then coexpressed the loader with FRB-NLuc-HA (hereafter named cargo) and determined the localization of each protein by confocal microscopy (recruitment assay). In the absence of the dimerizer, no colocalization was observed, the cargo showing a cytosolic pattern. Remarkably, in the presence of the dimerizer, a striking colocalization was observed (Figure 1C,D), the cargo being recruited to the CD63-positive endosomal compartments, a source of EVs.

https://doi.org/10.1021/acsabm.2c00955
ACS Appl. Bio Mater. 2023, 6, 1081−1091

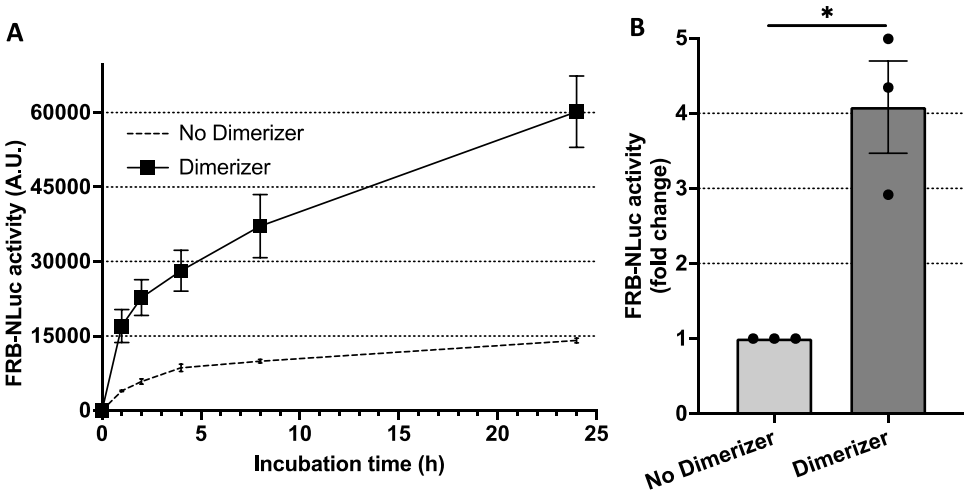

Figure 3. EV loading enhances the uptake and content delivery. (A) An uptake experiment was performed at different time points (1, 2, 4, 8, and 24 h) by incubating wild-type HeLa cells with EVs harboring both loader and FRB-NLuc-HA produced in the presence ("dimerizer") or not ("no dimerizer") of the A/C dimerizer. The FRB-NLuc-HA activity was normalized on the total protein input. Each dot corresponds to the mean of three independent technical duplicates. A.U., arbitrary unit. Mean ± SEM is represented. (B) A content delivery assay was performed by incubating wild-type HeLa cells for 24 h with EVs harboring both loader and FRB-NLuc-HA produced in the presence ("dimerizer") or not ("no dimerizer") of the A/C dimerizer. The FRB-NLuc-HA activity associated with the cytosolic fraction was measured. The fold change compared to the "no dimerizer" condition is represented. Each dot represents the mean of a technical duplicate. Mean ± SEM is represented. For statistical analysis, a Wilcoxon test was performed with $p < 0.05$ significant (*).

We then isolated EVs, produced in the absence or presence of the dimerizer, from donor cells transiently coexpressing the loader and the cargo. We used sequential centrifugation to roughly isolate EVs and then characterized their yield, size (by nanoparticle tracking analysis; NTA), composition (by Western blot), and the presence of the cargo (by luminescence). The addition of the dimerizer to the donor cells leads to no apparent differences in the particle diameter size (Figures 2A and S2), in the number of secreted EVs (Figure 2B), and in total EV protein concentration (Figure 2C). Also, no significant differences were observed for classical EV positive and negative markers: ALG-2-interacting protein X (ALIX), heat shock protein 70 (Hsp70), actin and cluster of differentiation 9 (CD9) as positive markers, and calnexin as a negative marker. This suggested that the dimerizer had no effect on EV formation (Figure 2D).

In contrast, in the absence of the dimerizer, we only observed a very weak luminescence (NLuc activity) in the EV fraction, whereas the addition of the dimerizer dramatically increased (3.5-fold) the luminescence, suggesting a dimerizer-induced cargo recruitment (Figure 2E).

To confirm the presence of the luminescent cargo in the EVs produced in the absence or presence of the dimerizer, we performed a floatation assay on sucrose gradient. Nine fractions were collected and analyzed by luminometry and Western blot. A pick of NLuc activity was observed in fraction 7 in both the presence and absence of the dimerizer. Here again, a weak activity was observed in the absence of the dimerizer, suggesting that a small portion of the overexpressed cargo is passively and inefficiently loaded into EVs, in accordance with previous observations.[4,6] Remarkably, the dimerizer increased the loading of the cargo by 4-fold (Figure 2F). Importantly, fraction 7 contained classical EV markers and was depleted of a negative marker such as trans-Golgi network glycoprotein 46 (TGN46) (Figure 2G). Furthermore, we virtually observed no NLuc activity and no detectable FRB signal in the last fraction, corresponding to the pellet, suggesting that the luminescent cargo is absent from any putative protein aggregates (Figure 2F,G).

These results showed that the EV loading system is efficient at recruiting a cytosolic cargo that would normally be absent or barely found in EVs.

EV Uptake and Cargo Delivery Characterization. Our previous study showed that only a small portion of EVs is uptaken by acceptor cells prior to releasing their soluble cargo (such as Hsp70) into their cytosol.[6,25] Our priority was therefore to test if the amount of the cargo loaded through our EV loading system was sufficient to enable a high level of EV uptake and cytosolic release within acceptor cells. EVs emanating from donor cells coexpressing the loader and the cargo treated or not with the dimerizer were incubated with wild-type Hela cells at different time points. Then, the NLuc activity associated with acceptor cells was analyzed by luminometry as a measure of EV uptake. Twenty-four hours after EV addition, a 4-fold increase of EV uptake was observed when EVs were actively loaded with the dimerizer (Figure 3A).

To assess if the positive effect on EV uptake was correlated with an improved cytosolic delivery, we performed a content delivery assay by cell fractionation at the 24 h time point, as described previously.[6,25] The cytosolic fraction was separated from membranes prior to measuring the luminescence. Remarkably, a 4-fold increase of cytosolic delivery was measured when EV loading was improved with the dimerizer (Figure 3B).

The biocompatibility of the loading system was also assessed by performing an Alamar blue assay on acceptor cells as a proxy of cell viability. Wild-type HeLa cells were incubated for 24 h with EVs harboring both loader and cargo produced in the presence or absence of the dimerizer. No condition significantly modified the cell viability compared to EV-naïve cells (Figure S3).

Together, these results showed that the EV loading system alone is capable of dramatically enhancing (4-fold increase) the

https://doi.org/10.1021/acsabm.2c00955
ACS Appl. Bio Mater. 2023, 6, 1081−1091

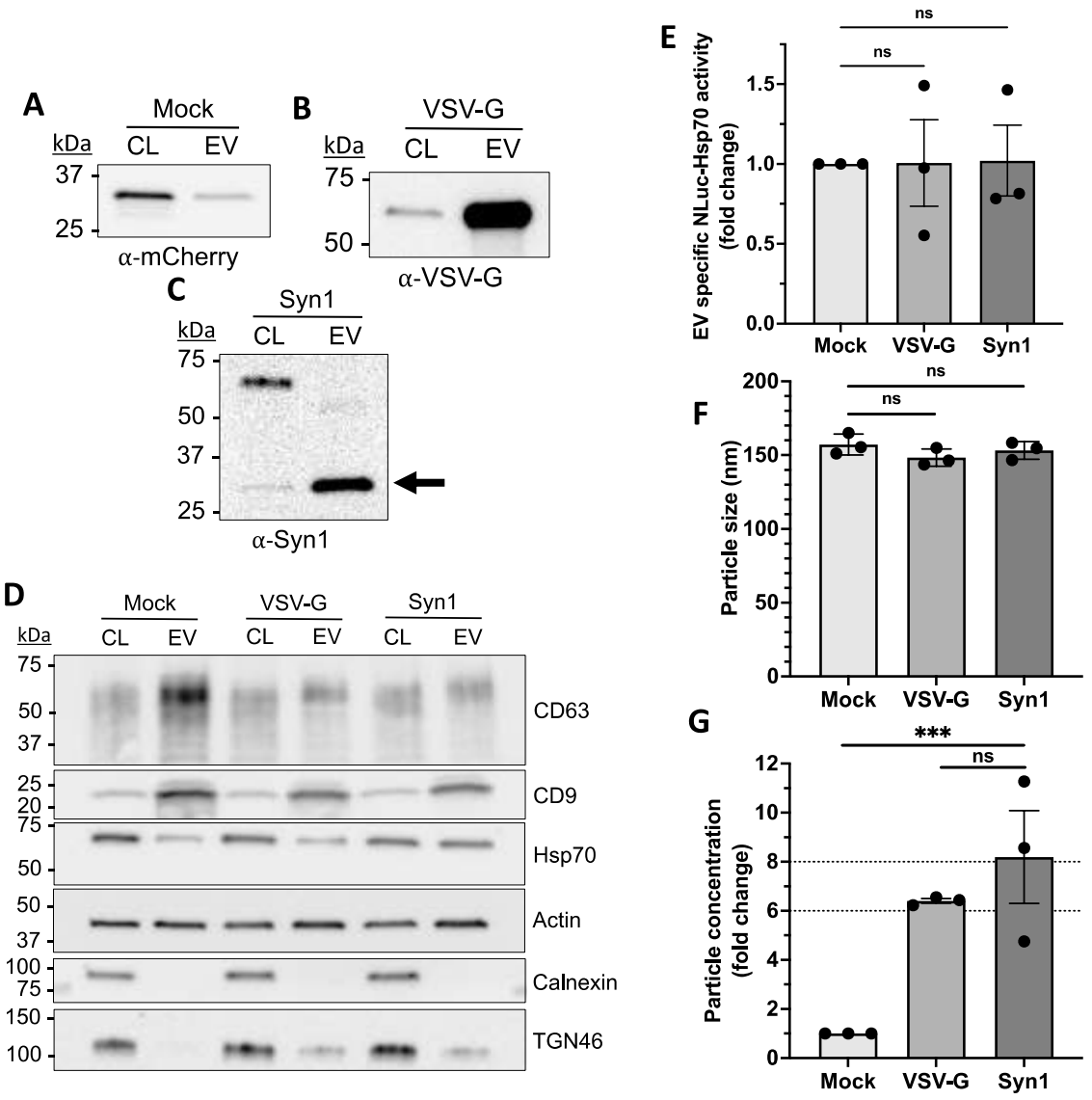

Figure 4. Fusogenic EV characterization. Cell lysates (CLs) and EVs from cells expressing mCherry ("Mock"), VSV-G, or Syn1 were analyzed by Western blot through different markers: (A) mCherry, (B) VSV-G, (C) Syn1, (D) CD63, CD9, Hsp70, actin, and calnexin. Equal amounts of protein were loaded. The black arrow in panel (C) represents the Syn1 surface subunit. (E) EV-associated NLuc-Hsp70 activity, (F) particle size, and (G) particle concentration were measured and plotted. All parameters, except particle size, were normalized on the "Mock" condition. Each dot represents the mean of a technical duplicate. Mean ± SEM is represented. For statistical analysis, a Kruskal–Wallis test was performed with $p \geq 0.05$ nonsignificant (ns) and $p < 0.005$ extremely significant (***).

final delivery of a cargo of interest within the cytosol of acceptor cells without harming them.

Development of a Virus-Free EV Fusion System. *EV Characterization.* Due to the aforementioned immunogenicity considerations, we looked for an alternative to VSV-G to improve the fusogenicity of our EVs. We focused on Syn1, a human fusogen responsible for cell–cell fusion during placenta formation.[20] We compared the properties of EVs emanating from cells stably expressing NLuc-Hsp70, a well-established soluble EV cargo,[6] and transfected with VSV-G, or Syn1, or a nonfusogenic control (mCherry).

mCherry (Mock condition) being only passively loaded into EVs was barely detectable in the EV fraction (Figure 4A), whereas VSV-G and Syn1 were both massively enriched in the EV fraction (Figure 4B,C). Note that Syn1 appeared as two bands: a higher band (around 60kDa) corresponding to nonmatured and noncleaved Syn1 and a lower band (around 33 kDa) corresponding to the extracellular "surface subunit" recognized by the antibody (amino acids 27–76; see the Materials and Methods section). Therefore, this Western blot suggested that the immature Syn1 remained predominantly in cells, while the mature and functional Syn1 is predominantly targeted to EVs (Figure 4C). In addition, classical EV positive and negative marker compositions were analyzed. No major differences were observed between the three conditions (Figure 4D). Abundance of the NLuc-Hsp70 cargo was also tested by luminometry and was shown to be similar in all conditions tested (Figure 4E). The EV size was also identical in all three conditions (Figures 4F and S4).

Interestingly, VSV-G or Syn1 expression strongly increased the particle release by donor cells by roughly 6-fold and 8-fold, respectively (Figure 4G). If this phenomenon was already described in the literature for VSV-G,[29] it had never been described for Syn1.

https://doi.org/10.1021/acsabm.2c00955
ACS Appl. Bio Mater. 2023, 6, 1081–1091

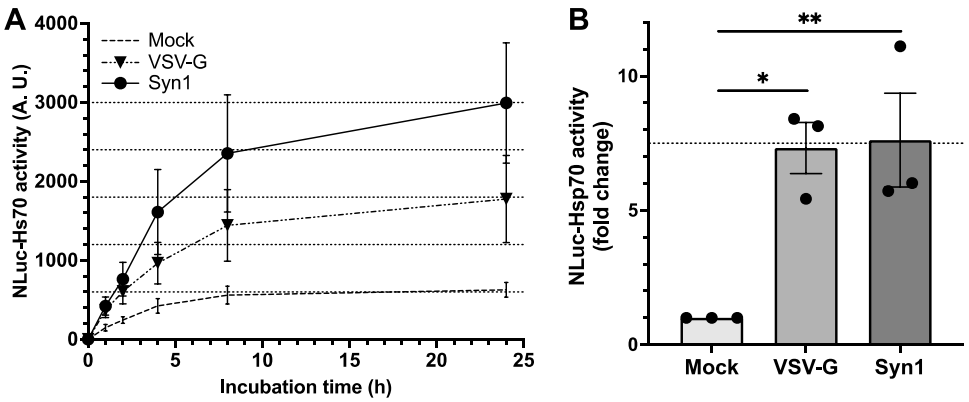

Figure 5. Fusogenic EVs enhance the uptake and content delivery. (A) An uptake experiment was performed at different time points (1, 2, 4, 8, and 24 h) by incubating wild-type HeLa cells with the same protein amounts of fusogenic EVs—produced from stable NLuc-Hsp70$^+$ HeLa—carrying mCherry ("Mock" condition) or harboring VSV-G or Syn1. Raw NLuc-Hsp70 activity is represented. Each dot corresponds to the mean of three independent technical duplicates. Mean ± SEM is represented. A.U., arbitrary unit. (B) A content delivery assay was performed by incubating wild-type HeLa cells for 24 h with fusogenic EVs—produced from stable NLuc-Hsp70$^+$ HeLa—harboring mCherry ("Mock" condition), VSV-G, or Syn1. NLuc-Hsp70 activity associated with the cytosolic fraction was measured. The fold change compared to the "Mock" condition is represented. Each dot represents the mean of a technical duplicate. Mean ± SEM is represented. For statistical analysis, a Kruskal–Wallis test was performed with $p < 0.05$ significant (*) and $p < 0.01$ very significant (**).

These results suggested that both fusion proteins were highly enriched on EVs without changing EV composition and size. Unexpectedly, they both increased EV release, which might be an advantage when considering EV biomanufacturing.

EV Uptake and Cargo Delivery Characterization. We then tested the uptake and delivery capacities of the fusogenic EVs and systematically compared Syn1 and VSV-G. First, VSV-G or Syn1 functionality was checked by monitoring syncytia formation by confocal microscopy, thus confirming the expression of VSV-G and Syn1 respective receptors on our acceptor cells (Figure S5).

The same amounts of NLuc-Hsp70-containing Mock EVs, VSV-G$^+$-EVs, or Syn1$^+$-EVs were then incubated with wild-type HeLa acceptor cells. Compared to control, Syn1$^+$-EVs increased both uptake and content delivery (5-fold at 24 h). Interestingly, the uptake of Syn1$^+$-EVs was 1.5-fold higher than the uptake of VSV-G$^+$-EVs (Figure 5A). However, this difference did not carry over to the cargo delivery step, which showed a similar efficiency for both fusogens (Figure 5B). This is perhaps due to the mechanistic differences between the two fusogens (surface binding, cell entry routes, fusion kinetics).[15,23]

An Alamar blue assay was conducted on wild-type HeLa incubated for 24 h with EVs containing mCherry or harboring VSV-G or Syn1. No significant differences were observed between the EV-naïve cells and the cells incubated with modified EVs, suggesting no negative effects on the acceptor cells (Figure S6).

These results showed that human Syn1 enhanced EV cargo delivery by 7.5-fold within acceptor cell cytosol without harming them, with a very similar efficiency to the viral VSV-G.

Development of Killer EVs. We decided to combine and apply our technologies—EV loading and fusion systems—to the oncotherapy field as a proof of concept. We focused on Diphtheria toxin, a very potent lethal toxin, that has been extensively investigated in the context of tumor ablation.[30] Interestingly, it has been shown that DTA, the catalytic subunit of the toxin, blocks protein synthesis and triggers cell death when expressed in the cytosol of the cell.[31]

However, DTA on its own does not cross the plasma membrane.[32] So far, virus-based[33] or liposome-based[34] vectors have been demonstrated to efficiently deliver DTA within infected cells and promote their death, but their therapeutic applications show limits, as it is the case for DTA-based immunotoxins.[30]

Taking advantage of the well-known mode of action of DTA, we first engineered DTA-resistant donor HT1080 cells by knocking down (KD) the diphtheria toxin resistance 2 (DPH2),[35] a gene responsible for diphthamide synthesis, which is absolutely required for DTA sensitivity.[36] We also engineered plasmids encoding FRB-DTA-HA and ensured that FRB-tagged DTA was still toxic for wild-type cells but not for cells knocked down for DPH2 (Figure S7).

We then isolated EVs from donor DPH2KD cells coexpressing the loader and FRB-DTA-HA treated or not with the dimerizer. We assessed the EV content by Western blot. As expected, $FKBP_2$-RFP-CD63 and CD9 were found in EVs, whereas calnexin was not. Remarkably, FRB-DTA-HA was only obviously detected in the EV fraction in the presence of the dimerizer (Figure 6A). This validated our loading system on a therapeutically relevant cargo.

Finally, we added Syn1 to the loading system and tested its impact on the delivery of the toxin to acceptor cells. Syn1 receptor expression at the plasma membrane of HT1080 acceptor cells was functionally checked through the cell–cell fusion assay (Figure S8).

To assess protein synthesis inhibition within acceptor cells, we took advantage of a short-lived GFP variant, named GFP-PEST.[37] We reasoned that EV-mediated DTA delivery should block or at least significantly decrease the GFP signal in the acceptor cells if protein synthesis is efficiently arrested (Figure 6B). Acceptor cells were then treated for 24 h with control vesicles (emanating from mock-transfected cells) or vesicles emanating from cells coexpressing $FKBP_2$-RFP-CD63 (loader) and FRB-DTA-HA, and Syn1 and treated or not with the dimerizer. In the absence of the dimerizer, fusogenic Syn1$^+$-EVs that contain a no-to-barely detectable level of DTA (Figure 6A) had no or only minor effect on the GFP-PEST signal and cell counting (around 15% for both parameters as

https://doi.org/10.1021/acsabm.2c00955
ACS Appl. Bio Mater. 2023, 6, 1081–1091

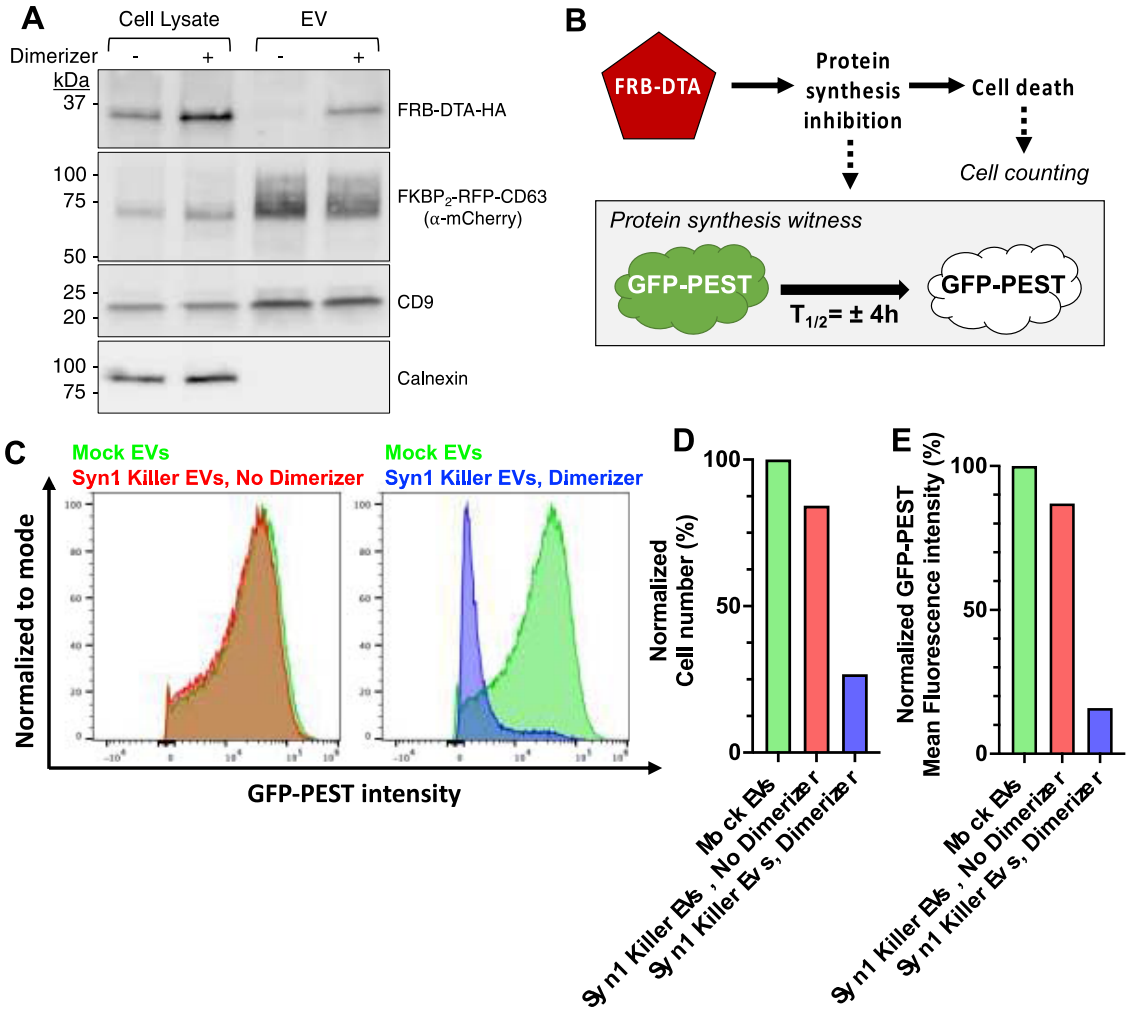

Figure 6. Loader$^+$/Syn1$^+$-EVs recruit FRB-DTA-HA and kill acceptor cells. (A) Cell lysates and EVs coexpressing FRB-DTA-HA and FKBP$_2$-RFP-CD63 from DPH2KD HeLa cells treated ("+") or not ("−") with the A/C dimerizer drug were analyzed by Western blot. (B) DTA inhibits protein synthesis, which leads to cell death. Protein synthesis inhibition is monitored through GFP-PEST fluorescence. (C) A killing assay was performed incubating GFP-PEST HT1080 acceptor cells with Mock EVs and killer EVs (loader$^+$/Syn1$^+$-EVs) produced in the presence ("dimerizer") or absence ("no dimerizer") of the A/C dimerizer drug. The acceptor cells were analyzed by FACS after 24 h of EV incubation. Green fluorescence was analyzed by FACS, and data for each EV-treated sample was plotted against PBS-treated cells. (D) Cell counting and (E) GFP-PEST mean fluorescence intensity were plotted. (C−E) Green, Mock EVs; red, loader$^+$/Syn1$^+$-EVs without dimerizer; blue, loader$^+$/Syn1$^+$-EVs with dimerizer.

judged by FACS analysis) when compared to cells treated with mock EVs (Figure 6C−E). Remarkably, when EVs were produced in the presence of the dimerizer, those fusogenic Syn1$^+$/loader$^+$ EVs efficiently killed 74% of the acceptor cells (Figure 6D) and triggered a strong decrease of the GFP-PEST signal in 85% of the remaining acceptor cells (Figure 6E). In other words, these EVs successfully delivered their content within the cytosol of 96% of the initial acceptor cell population.

Altogether, these results suggested an absolute requirement of both loading system and Syn1-based fusion system to functionalize killer EVs at a level that would be compatible with therapeutic applications.

DISCUSSION

Loading System. Here, we propose a two-step method to independently control EV cargo loading and EV cargo delivery through the activation of membrane fusion without the use of viral components, which has long represented a burden for the biosafety regulation in the manufacturing of delivery vectors.[9] After rigorously assessing the *ex vivo* efficiency of each method through the use of luciferase-based reporters, we show that this two-step process enables the massive killing of acceptor cells when EVs are equipped with a lethal toxin. These virus-free killer EVs may open new possibilities in tumor treatment.

Concerning the loading strategy, we choose the flexibility of a drug-inducible reversible system. Note that during the completion of this study similar systems have been used to load cargo within EVs (using CD63 or other tetraspanins) or virus-like particles.[11−14] Unsatisfyingly, the outcomes of those studies were very different. In brief, cargo loading successes ranged from no increase (Osteikoetxea et al.[14] when using CD9) to a 100-fold increase (Somiya et al.[13] when using CD81) over the background. Although we cannot formally explain all of the causes for these apparent discrepancies, we noticed significant differences between the studies that refer to (i) the loading design, (ii) the nature of the dimerization drug (rapamycin or analog), (iii) the cargo nature and basal expression, and (iv) the methods of detection and analysis.

In some studies,[13] FKBP was fused to the carboxyterminal extremity of CD63, which also contains its endosomal

https://doi.org/10.1021/acsabm.2c00955
ACS Appl. Bio Mater. 2023, 6, 1081−1091

targeting signal.[38] This might affect the localization of the protein. Here, we tagged the N-terminal part of CD63 and showed that the chimeric protein is properly localized (Figures 1B and S1). We also used two repeats of FKBP, which was proposed to optimize the dimerization *in vitro* by increasing ligand avidity.[39] We moreover used a mutant form of the FRB domain (T2098L) that allows its dimerization with AP21967 (renamed A/C dimerizer), the rapamycin analog used in this study. This version is less bioactive than rapamycin and nontoxic to cells up to 1 μM.[27] This system permits EV loading without interfering with the mTOR pathway, whereas other studies used the endogenous sequence of the FRB domain and rapamycin, which may have direct and indirect impacts on the dimerization and cell signaling. In addition, we used here NanoLuciferase-tagged cargo to acutely measure the amount of cargo within isolated EVs through bulk luminescence measurement. NLuc allows a highly sensitive and direct measurement.[6,25] This indeed allows us to detect EV uptake and content delivery even without loading or fusion systems (Figures 3 and 5), which was not possible in other studies. In other reports, EV cargo loading was assessed through immunoblot,[12,14] which is less sensitive and only semiquantitative, or through split luciferase complementation,[13] which could be biased by a high LgBiT background signal. Also, some studies assessed indirectly EV loading efficiency by monitoring cargo release via reporter gene assays.[11] Finally, we confirmed our data using EVs isolated by floatation, which ruled out any involvement of contaminants such as protein aggregates. This validates EVs as the delivery vector.

Fusion System. Concerning the fusion/delivery system, we established here that Syn1 is a novel nonviral alternative to VSV-G. The Syn1 receptor is, much like the VSV-G receptor, widely expressed in tissues.[40] This positions Syn1 as an excellent candidate to replace VSV-G as the next gold standard for DDS. In addition, Syn1 does not require EV internalization and endosomal acidification within the target cell for efficient fusion, which may facilitate EV-mediated therapeutics delivery and avoid their lysosomal degradation. Segel et al. recently showed that Syncytin-A (the Syn1 murine ortholog) could be used to package and deliver mRNA with PEG10 (paternally expressed gene 10 protein) as capsid.[41] Nevertheless, the fact that human Syn1 could be used to engineer bioactive EVs had never been shown before our study, especially in the context of protein delivery. *In vivo* experiments will, however, be required to further assess the potency of Syn1$^+$-EVs as a therapeutics vector.

Finally, Syncytin-2 (Syn2) also has demonstrated fusogenic capacities.[42] Interestingly, its cognate receptor (major facilitator superfamily domain-containing protein 2, MFSD2A) has a different expression pattern than the Syn1 receptor (ASCT2). Notably, MFSD2A is enriched on activated CD8$^+$ T cells[43] and is necessary for the blood−brain barrier homeostasis.[44] Thus, Syn2 could constitute the next tool to efficiently reach challenging targets such as the brain or lymphocytes.

Killer EVs. DTA has long been considered a good candidate for tumor ablation therapy, but the lack of efficient mode of administration minimized its application.[30] We clearly established here, *ex vivo*, that our two-step process efficiently triggers the elimination of acceptor cells. This suggests a path to manufacture virus-free killer EVs, specialized in tumor ablation. Of course, our initial attempt will require further development that includes *in vivo* validation and specific cell targeting to ultimately validate killer EVs and other therapeutical EVs.

CONCLUSIONS

We developed here a two-step process to enhance dramatically EV protein cargo loading and delivery within the acceptor cell cytosol. First, the loading system led to at least a 4-fold increase of EV cargo loading, resulting in a similar increase of the downstream EV cargo delivery. Then, we used Syncytin-1 to replace viral proteins, which led to a >5-fold increase of the EV uptake and content delivery. Syncytin-1 appears to be at least as efficient as VSV-G, and an excellent candidate for humanized delivery vector.

Both methods can be used in synergy to deliver more efficient protein cargo. As an illustration, we used the FRB-DTA as a lethal cargo to kill acceptor cancer cells. We reached 75% of efficiency to kill acceptor cells when using loading and Syncytin-1 in synergy and successfully affected 96% of them. This is at least as efficient as VSV-G-mediated delivery of the same toxin encapsulated by EVs.[35]

Altogether, these results could have a major impact on the development of new generations of therapies. Indeed, while previous studies already focused on single-step strategies to bioengineer EVs, our results suggest that a combination of methods that control cargo loading and delivery synergistically improves EV functionalization. We use here DTA as a proof of concept first cargo of interest, but the versatility of the system enables us to load any protein-based therapeutics, such as the genome editing toolbox (Cas9/guide RNA). Adding a targeting step to achieve specific cell targeting will surely extend the potency of future EV-based delivery vectors.

MATERIALS AND METHODS

Cell Culture and Transfection. HeLa cells—wild-type (from ATCC, VA) and genetically modified—GFP-PEST HT1080 (generated previously in our laboratory[35]), HEK293T (from ATCC, VA), and SW480 (gift from Corinne Quittau-Prévostel, from ATCC, VA) cells were grown in DMEM GlutaMAX (Gibco, IL) supplemented with 10% FBS at 37 °C at 5% CO_2. HT1080 cell medium was further complemented with MEM NEAA (Gibco, IL). EGI-1 cells (gift from Laura Fouassier and Nicolas Kuszla, from ATCC, VA) were grown in DMEM 1× + GlutaMAX-1, 1 g/L D-glucose ("low sucrose") + pyruvate (21885-025, Gibco, IL) supplemented with 10% FBS, 100 UI/L of penicillin, 100 μg/mL of streptomycin, and 10 mmol/L of HEPES. HeLa stably expressing NanoLuciferase-Hsp70 was generated in our laboratory,[6] as well as DPH2KD HeLa cells[35] according to Picco et al.[36] HeLa stably expressing CD8-GFP was selected with hygromycin B (50 mg/mL, Invitrogen, MA) after lipofectamine 2000 transfection. Cells were transfected at a 70% confluency with lipofectamine 2000 (Invitrogen, MA) according to the manufacturer's instructions.

Plasmids. pC_4-mCherry-HA has been previously described.[45] VSV-G was purchased from Addgene (#8454). Syncytin-1 was a generous gift from Thierry Heidmann. pC_4-FRB-HA corresponds to pC_4-R_HE (Takara Bio Inc., Shiga, Japan). pC_4-$FKBP_2$-HA was generated by digesting pC_4-R_HE and pC_4M-F2E (Takara Bio Inc., Shiga, Japan) with *Xba*I and *Spe*I, and swapping $FKBP_2$ into empty pC_4-R_HE. pC_4-$FKBP_2$-RFP-CD63 was generated by amplifying RFP-CD63 (a generous gift from Walther Mothes) with the following primers: (forward) GCAGCATCTAGAATGGCCTCCTCCGAG-GACGTC and (reverse) GCAGCAGGATCCCTTCTACAT-CACCTCGTA-GCCACTTCTG, and inserting it into pC_4-$FKBP_2$-HA digested with *Eco*RI and *Bam*HI. pC_4-FRB-NLuc-HA was generated by amplifying NLuc (from NLuc-Hsp70[6]) with the following primers: (forward) GCAGCATCTAGAATGGTCTTCA-

https://doi.org/10.1021/acsabm.2c00955
ACS Appl. Bio Mater. 2023, 6, 1081−1091

CACT-CGAAGATTTCGTTG and (reverse) GCAGCAACTAG-TCGCCAGAATGCGTTCGCAC, and inserting it into pC_4-R_HE using the *Spe*I restriction site. CD8-GFP was purchased from Addgene (#86051), digested with *Nhe*I and *Xba*I, and inserted into pcDNA3-smURFP-IRES-eGFP (Addgene, #80343). FRB-DTA-HA was generated as follows: FRB was cloned into pcDNA3.1(+) (#V70020, Invitrogen, MA) with *Nhe*I/*Bam*HI using (forward) GCTGCAGCTAGCGATCG-CCATGGTGGC, and (reverse) TGCAGCGGATCCACCGC-TCGAGCCTCCAC; DTA-HA[35] was cloned into it with *Bam*HI and *Xba*I by using (forward) GCTGCAGGATCCATGG-ATGATGTTGTTGATTCTTC-TAAATC and (reverse) TGC-AGCTCTAGACTTATG-CGTAATCTGGTACG.

EV Isolation. Six hours post transfection, EV donor cells were transferred in serum starvation medium (DMEM GlutaMAX, 5 mL per 10 cm dish) supplemented or not with the A/C heterodimerizer drug (Takara Bio Inc., Shiga, Japan). Conditioned medium was harvested 24 h later for EV preparation and was first centrifuged for 20 min at 2000*g* at 4 °C to remove dead cells and debris, then 30 min at 10 000*g* at 4 °C (45Ti rotor, Optima XE-90 Ultracentrifuge, Beckman Coulter, CA) to remove large vesicles and apoptotic bodies, and then 1 h and 30 min at 100 000*g* at 4 °C (45Ti rotor, Optima XE-90 Ultracentrifuge, Beckman Coulter, CA) to isolate EVs. Finally, the 100 000*g* pellet was washed in PBS and centrifuged for 1 h and 10 min at 100 000*g* at 4 °C (SW55 rotor, Optima XE-90 Ultracentrifuge, Beckman Coulter, CA). The final pellet was resuspended in PBS and used immediately or stored at 4 °C for 24 h maximum.

Floatation Assay. EV isolation was performed without the washing step. The 100 000*g* pellet was resuspended in 1 mL of 60% sucrose in PBS[46] and deposited at the bottom of an SW55 tube (Beckman Coulter, CA). One milliliter of 30% sucrose in PBS and then 1 mL of PBS were successively deposited above. Samples were then centrifuged for at least 15 h at 100 000*g* at 4 °C (SW55 rotor, Optima XE-90 Ultracentrifuge, Beckman Coulter, CA) and then recovered into nine fractions of 300 μL from top to bottom of the gradient. Luminescence activity of each fraction was directly measured. Each fraction was then diluted into 4 mL of PBS and centrifuged for 1 h at 100 000*g* at 4 °C (MLA-50 rotor, Optima MAX-XP Ultracentrifuge, Beckman Coulter, CA) to wash out the sucrose and perform Western blotting. At this step, fractions 1 and 2 were pooled.

NanoLuciferase-Based Uptake Assay and Content Delivery Assay. These assays were performed as described previously[6,25] with EVs carrying an FRB-NanoLuciferase-HA or NanoLuciferase-Hsp70 as luminescent cargo. The NanoLuciferase activity was assayed using the Nano-Glo Luciferase Assay System (Promega, WI) and the iD3 SpectraMax microplate reader (Molecular Devices, CA).

Recruitment Assay. Cells were seeded at day 0 on glass coverslips and were cotransfected the next day with pC4-$FKBP_2$-RFP-CD63 and pC4-FRB-NLuc-HA with a 1:2.3 ratio. On day 3, the cells were treated or not with the A/C heterodimerizer drug (Takara Bio Inc., Shiga, Japan) for 1 h at 37 °C and then prepared for confocal microscopy observation. FRB-NLuc-HA was labeled for immunofluorescence as described below in the Confocal Microscopy section.

Fusion Assay. HeLa CD8-GFP or HT1080 cells were seeded at day 0 on glass coverslips. On day 1, cells were transfected with an empty vector ("Mock" condition), VSV-G (only HeLa cells), or Syn1 plasmids. For HeLa cells, at day 2, each condition was treated or not with fusion buffer (10 mM Na_2HPO_4, 150 mM NaCl, 10 mM MES, 10 mM HEPES, adjusted to pH 5.5) for 1 min and then incubated in their culture media for 1 h before fixation. Cells and syncytia were observed by confocal microscopy.

Antibodies. Primary antibodies: Anti-TGN46 (PA5-23068, Invitrogen, MA), Anti-hCD9 (Clone MM2-57, Millipore, MA), Anti-hCD63 (556019, BD Biosciences, New Jersey), Anti-HA (for IF, 66006-2-Ig, Proteintech, IL; for WB, C29F4, Cell Signaling, MA), Anti-Cherry (5993-100, BioVision, CA), Anti-calnexin (ab133615, Abcam, Cambridge, U.K.), Anti-ALIX (Clone 3A9, 2171S, Cell Signaling, MA), Anti-HSP70/HSP72 (Clone C92F3A-5, ADI-SPA-810F, Enzo Life Sciences, NY), Anti-Actin (Clone C4, MAB1501, Millipore, MA), Anti-VSV-G (Clone P5D4, CurieCoreTech of Curie Institute, Paris, France), and Anti-Syncytin-1 (recognizes amino acids 27−76; ab179693, Abcam, Cambridge, U.K.). Secondary antibodies for Western blotting: goat anti-rabbit IgG (H + L)-HRP conjugate (1706515, Bio-Rad, CA) and goat antimouse IgG (H + L)-HRP conjugate (1706516, Bio-Rad, CA). Secondary antibody for immunofluorescence: goat antimouse IgG (H + L) highly cross-absorbed secondary antibody, Alexa Fluor 488 (A11029, Thermo Fisher Scientific, IL).

Western Blotting. Cells were collected and washed in PBS; the pellet was resuspended in lysis buffer (50 mM tris−HCl, 150 mM NaCl, 1% Triton-X100, protease/phosphatase inhibitor cocktail (Roche, Switzerland), pH 8) for a 20 min incubation on ice and then centrifuged for 15 min at 20 000*g* at 4 °C, and the supernatant was collected as the cell lysate. Cell lysates and EV protein concentrations were assayed with the Micro-BCA Protein Assay Kit (Thermo Scientific, IL). Samples were mixed with 4× Laemmli buffer (Bio-Rad, CA) completed with 10% β-mercaptoethanol (BME), except when immunoblotting for CD63 (BME was not added in this case). Electrophoresis was performed on 4−20% polyacrylamide gels (Bio-Rad, CA) in tris/glycine/SDS buffer (Bio-Rad, CA), and proteins were transferred on immunoblot PVDF membranes (0.2 μm, Bio-Rad, CA) using the TransBlot Turbo system (Bio-Rad, CA). The Precision Plus Protein Standards (Bio-Rad, CA) was used as a protein weight ladder. Membranes were then blocked with 0.05% Tween, 5% milk in PBS for 1 h at room temperature, and incubated overnight at 4 °C with the primary antibody diluted at 1/1000 in 0.05% Tween, 5% milk in PBS. Membranes were then washed for 1 h in PBS 0.05% Tween, incubated with secondary antibodies diluted at 1/10 000 in PBS 0.05% Tween, and washed for 1 h in PBS 0.05% Tween. Membranes were revealed using the Clarity Western ECL Substrate (Bio-Rad, CA) and the ImageQuant LAS 400 imager (GE Healthcare Life Sciences, Chicago). Image analysis and quantification were performed using the Fiji software.

Confocal Microscopy. Cells were either seeded on glass coverslips 1 day before fixation for stable cell lines or seeded 2 days before and transfected the next day for transiently transfected cells. Cells were then washed 3 times with cold PBS and incubated in 4% PFA in PBS for 15 min at room temperature. If antibody labeling was performed for immunofluorescence, cells were then permeabilized with 0.1% Triton-X100 (Sigma-Aldrich, MA) for 15 min at room temperature, incubated with primary antibody diluted at 1/500 for 2 h at room temperature, and then with secondary antibody diluted at 1/2000 for 1 h at room temperature. Finally, a DAPI staining was performed when needed at 0.5 μg/mL. Coverslips were mounted with a ProLong Diamond Antifade Mountant (Invitrogen). Images were acquired using an LSM 880 confocal microscope with a 63× oil immersion objective (ZEISS, Baden-Württemberg, Germany). Image analysis and quantification were performed using the Fiji software.

Nanoparticle Tracking Analysis. NTA was performed using the ZetaView x20 (Particle Metrix, Ammersee, Germany) with the following parameters: laser 488 nm, scatter, 11 positions, 1 cycle, sensitivity 80, shutter 100, pH = 7 entered, *T* °C sensed. All samples were diluted into filtered PBS.

Alamar Blue Assay. An uptake assay was performed over 24 h of incubation. The alamarBlue HS Cell Viability Reagent (Invitrogen, MA) was added to the medium 2 h before the end of incubation according to the constructor protocol. For "Cell + Triton 0.05%" condition, Triton-X100 (Sigma-Aldrich, MA) was added at this step. After 2 h in the Alamar blue reagent, the signal was measured by fluorescence (excitation at 545 nm, emission at 590 nm) using the iD3 SpectraMax microplate reader (Molecular Devices, CA).

Killing Assay. EVs were prepared from DPH2KD cells transfected with $FKBP_2$-RFP-CD63, FRB-DTA-HA, and Syn1 and cultivated with or without the dimerizer drug. Each EV (100 μg/mL) was applied to GFP-PEST HT1080 cells. Twenty-four hours after EV treatment, acceptor cells were washed and detached with 0.05% trypsin-EDTA, washed in PBS, and pelleted for 5 min at 1000*g* at 4 °C. Cells were then resuspended in PBS and analyzed on an Attune NxT flow cytometer (Thermo Scientific, IL). Samples were incubated with 10

https://doi.org/10.1021/acsabm.2c00955
ACS Appl. Bio Mater. 2023, 6, 1081−1091

μg/mL of DAPI (Merck Millipore, MA) right before analysis. The gating strategy is depicted in Figure S7. Analysis was performed using the FlowJo software (BD Bioscience, New Jersey).

Statistical Analysis. Nonparametric tests were used in this paper. For loading experiments, a Wilcoxon test was performed, and for fusion experiments, a Kruskal–Willis test was performed using GraphPad Prism version 9.5.0. Source data are reported in the Supporting Information.

■ ASSOCIATED CONTENT

Supporting Information

The Supporting Information is available free of charge at https://pubs.acs.org/doi/10.1021/acsabm.2c00955.

Additional experiments including EV size profile, fusion assay, Alamar blue assays, cell line generation, and FACS gating strategy (PDF)

Charts and histogram source data (XLSX)

■ AUTHOR INFORMATION

Corresponding Author

Gregory Lavieu − *INSERM U1316, CNRS UMR 7057, Université Paris Cité, 75006 Paris, France;* orcid.org/0000-0001-9852-4977; Email: gregory.lavieu@inserm.fr

Authors

Sheryl Bui − *INSERM U1316, CNRS UMR 7057, Université Paris Cité, 75006 Paris, France;* orcid.org/0000-0002-7460-6676

Julia Dancourt − *INSERM U1316, CNRS UMR 7057, Université Paris Cité, 75006 Paris, France*

Complete contact information is available at: https://pubs.acs.org/10.1021/acsabm.2c00955

Author Contributions

S.B. and J.D. participated in the design of the experiments, performed the experiments, and analyzed the data; G.L. supervised the project; and S.B., J.D., and G.L. wrote and edited the manuscript.

Notes

The authors declare no competing financial interest.

■ ACKNOWLEDGMENTS

The authors thank Thierry Heidmann (Gustave Roussy Institute) for donating the Syncytin-1 plasmid and Walter Mothes (Yale School of Medicine) for the RFP-CD63 plasmid, Laura Fouassier and Nicolas Kuszla for donating the EGI-1 cells, Corinne Quittau-Prévostel for the SW480 cells, the microscopy and Cyto2BM (from Biomedtech) facilities of the CUSP, and Clément Hua for his advice for statistical analysis. S.B. is a recipient of a Ph.D. fellowship from Paris Sciences & Lettres (PSL) University. This work was supported by INSERM, French National Research Agency (Excelldisc, BIOEV, EVfusion), and Chaire d'Excellence Idex, Université Paris Cité.

■ ABBREVIATIONS

ASCT2, alanine serine cysteine transporter 2; CD9, cluster of differentiation 9; CD63, cluster of differentiation 63; CL, cell lysate; COI, cargo of interest; DDS, drug delivery system; DPH2, diphthamide biosynthesis 2; DPH2, diphtheria toxin resistance 2; DTA, diphtheria toxin A; EVs, extracellular vesicles; FKBP, FK506 binding protein; FRB, FKBP-rapamycin binding; GFP, green fluorescent protein; Hsp70, heat shock protein 70; KD, knockdown; MFSD2A, major facilitator superfamily domain-containing protein 2A; NLuc, Nano-Luciferase; NTA, nanoparticle tracking analysis; RFP, red fluorescent protein; Syn1, Syncytin-1; TGN46, trans-Golgi network glycoprotein 46; VSV-G, vesicular stomatitis virus glycoprotein; WT, wild-type

■ REFERENCES

(1) Mathieu, M.; Martin-Jaular, L.; Lavieu, G.; Théry, C. Specificities of Secretion and Uptake of Exosomes and Other Extracellular Vesicles for Cell-to-Cell Communication. *Nat. Cell Biol.* **2019**, *21*, 9−17.

(2) Vader, P.; Mol, E. A.; Pasterkamp, G.; Schiffelers, R. M. Extracellular Vesicles for Drug Delivery. *Adv. Drug Delivery Rev.* **2016**, *106*, 148−156.

(3) Alvarez-Erviti, L.; Seow, Y.; Yin, H.; Betts, C.; Lakhal, S.; Wood, M. J. A. Delivery of SiRNA to the Mouse Brain by Systemic Injection of Targeted Exosomes. *Nat. Biotechnol.* **2011**, *29*, 341−345.

(4) Le Saux, S.; Aubert-Pouëssel, A.; Mohamed, K. E.; Martineau, P.; Guglielmi, L.; Devoisselle, J.-M.; Legrand, P.; Chopineau, J.; Morille, M. Interest of Extracellular Vesicles in Regards to Lipid Nanoparticle Based Systems for Intracellular Protein Delivery. *Adv. Drug Delivery Rev.* **2021**, *176*, No. 113837.

(5) Couch, Y.; Buzàs, E. I.; Di Vizio, D.; Gho, Y. S.; Harrison, P.; Hill, A. F.; Lötvall, J.; Raposo, G.; Stahl, P. D.; Théry, C.; Witwer, K. W.; Carter, D. R. F. A Brief History of Nearly EV-Erything - The Rise and Rise of Extracellular Vesicles. *J. Extracell. Vesicles* **2021**, *10*, No. e12144.

(6) Bonsergent, E.; Grisard, E.; Buchrieser, J.; Schwartz, O.; Théry, C.; Lavieu, G. Quantitative Characterization of Extracellular Vesicle Uptake and Content Delivery within Mammalian Cells. *Nat. Commun.* **2021**, *12*, No. 1864.

(7) Joshi, B. S.; de Beer, M. A.; Giepmans, B. N. G.; Zuhorn, I. S. Endocytosis of Extracellular Vesicles and Release of Their Cargo from Endosomes. *ACS Nano* **2020**, *14*, 4444−4455.

(8) Somiya, M.; Kuroda, S. Real-Time Luminescence Assay for Cytoplasmic Cargo Delivery of Extracellular Vesicles. *Anal. Chem.* **2021**, *93*, 5612−5620.

(9) Herrmann, I. K.; Wood, M. J. A.; Fuhrmann, G. Extracellular Vesicles as a Next-Generation Drug Delivery Platform. *Nat. Nanotechnol.* **2021**, *16*, 748−759.

(10) Piffoux, M.; Volatron, J.; Cherukula, K.; Aubertin, K.; Wilhelm, C.; Silva, A. K. A.; Gazeau, F. Engineering and Loading Therapeutic Extracellular Vesicles for Clinical Translation: A Data Reporting Frame for Comparability. *Adv. Drug Delivery Rev.* **2021**, *178*, No. 113972.

(11) Gee, P.; Lung, M. S. Y.; Okuzaki, Y.; Sasakawa, N.; Iguchi, T.; Makita, Y.; Hozumi, H.; Miura, Y.; Yang, L. F.; Iwasaki, M.; Wang, X. H.; Waller, M. A.; Shirai, N.; Abe, Y. O.; Fujita, Y.; Watanabe, K.; Kagita, A.; Iwabuchi, K. A.; Yasuda, M.; Xu, H.; Noda, T.; Komano, J.; Sakurai, H.; Inukai, N.; Hotta, A. Extracellular Nanovesicles for Packaging of CRISPR-Cas9 Protein and SgRNA to Induce Therapeutic Exon Skipping. *Nat. Commun.* **2020**, *11*, No. 1334.

(12) Campbell, L. A.; Coke, L. M.; Richie, C. T.; Fortuno, L. V.; Park, A. Y.; Harvey, B. K. Gesicle-Mediated Delivery of CRISPR/Cas9 Ribonucleoprotein Complex for Inactivating the HIV Provirus. *Mol. Ther.* **2019**, *27*, 151−163.

(13) Somiya, M.; Kuroda, S. Engineering of Extracellular Vesicles for Small Molecule-Regulated Cargo Loading and Cytoplasmic Delivery of Bioactive Proteins. *Mol. Pharmaceutics* **2022**, *19*, 2495−2505.

(14) Osteikoetxea, X.; Silva, A.; Lázaro-Ibáñez, E.; Salmond, N.; Shatnyeva, O.; Stein, J.; Schick, J.; Wren, S.; Lindgren, J.; Firth, M.; Madsen, A.; Mayr, L. M.; Overman, R.; Davies, R.; Dekker, N. Engineered Cas9 Extracellular Vesicles as a Novel Gene Editing Tool. *J. Extracell. Vesicles* **2022**, *11*, No. e12225.

(15) Munis, A. M.; Bentley, E. M.; Takeuchi, Y. A Tool with Many Applications: Vesicular Stomatitis Virus in Research and Medicine. *Expert Opin. Biol. Ther.* **2020**, *20*, 1187−1201.

(16) Clague, M. J.; Schoch, C.; Zech, L.; Blumenthal, R. Gating Kinetics of PH-Activated Membrane Fusion of Vesicular Stomatitis Virus with Cells: Stopped-Flow Measurements by Dequenching of Octadecylrhodamine Fluorescence. *Biochemistry* **1990**, *29*, 1303−1308.
(17) Fredericksen, B. L.; Whitt, M. A. Mutations at Two Conserved Acidic Amino Acids in the Glycoprotein of Vesicular Stomatitis Virus Affect PH-Dependent Conformational Changes and Reduce the PH Threshold for Membrane Fusion. *Virology* **1996**, *217*, 49−57.
(18) Munis, A. M.; Mattiuzzo, G.; Bentley, E. M.; Collins, M. K.; Eyles, J. E.; Takeuchi, Y. Use of Heterologous Vesiculovirus G Proteins Circumvents the Humoral Anti-Envelope Immunity in Lentivector-Based In Vivo Gene Delivery. *Mol. Ther. Nucleic Acids* **2019**, *17*, 126−137.
(19) Power, A. T.; Wang, J.; Falls, T. J.; Paterson, J. M.; Parato, K. A.; Lichty, B. D.; Stojdl, D. F.; Forsyth, P. A. J.; Atkins, H.; Bell, J. C. Carrier Cell-Based Delivery of an Oncolytic Virus Circumvents Antiviral Immunity. *Mol. Ther.* **2007**, *15*, 123−130.
(20) Blond, J. L.; Lavillette, D.; Cheynet, V.; Bouton, O.; Oriol, G.; Chapel-Fernandes, S.; Mandrand, B.; Mallet, F.; Cosset, F. L. An Envelope Glycoprotein of the Human Endogenous Retrovirus HERV-W Is Expressed in the Human Placenta and Fuses Cells Expressing the Type D Mammalian Retrovirus Receptor. *J. Virol.* **2000**, *74*, 3321−3329.
(21) Tolosa, J. M.; Schjenken, J. E.; Clifton, V. L.; Vargas, A.; Barbeau, B.; Lowry, P.; Maiti, K.; Smith, R. The Endogenous Retroviral Envelope Protein Syncytin-1 Inhibits LPS/PHA-Stimulated Cytokine Responses in Human Blood and Is Sorted into Placental Exosomes. *Placenta* **2012**, *33*, 933−941.
(22) Cheynet, V.; Ruggieri, A.; Oriol, G.; Blond, J.-L.; Boson, B.; Vachot, L.; Verrier, B.; Cosset, F.-L.; Mallet, F. Synthesis, Assembly, and Processing of the Env ERVWE1/Syncytin Human Endogenous Retroviral Envelope. *J. Virol.* **2005**, *79*, 5585−5593.
(23) Lavillette, D.; Marin, M.; Ruggieri, A.; Mallet, F.; Cosset, F.-L.; Kabat, D. The Envelope Glycoprotein of Human Endogenous Retrovirus Type W Uses a Divergent Family of Amino Acid Transporters/Cell Surface Receptors. *J. Virol.* **2002**, *76*, 6442−6452.
(24) Rankin-Turner, S.; Vader, P.; O'Driscoll, L.; Giebel, B.; Heaney, L. M.; Davies, O. G. A Call for the Standardised Reporting of Factors Affecting the Exogenous Loading of Extracellular Vesicles with Therapeutic Cargos. *Adv. Drug Delivery Rev.* **2021**, *173*, 479−491.
(25) Bonsergent, É.; Bui, S.; Lavieu, G. Quantitative Measurement of Extracellular Vesicle Content Delivery Within Acceptor Cells. *Methods Mol. Biol.* **2022**, *2473*, 397−403.
(26) Rivera, V. M.; Clackson, T.; Natesan, S.; Pollock, R.; Amara, J. F.; Keenan, T.; Magari, S. R.; Phillips, T.; Courage, N. L.; Cerasoli, F.; Holt, D. A.; Gilman, M. A Humanized System for Pharmacologic Control of Gene Expression. *Nat. Med.* **1996**, *2*, 1028−1032.
(27) Pollock, R.; Issner, R.; Zoller, K.; Natesan, S.; Rivera, V. M.; Clackson, T. Delivery of a Stringent Dimerizer-Regulated Gene Expression System in a Single Retroviral Vector. *Proc. Natl. Acad. Sci. U.S.A.* **2000**, *97*, 13221−13226.
(28) Kowal, J.; Arras, G.; Colombo, M.; Jouve, M.; Morath, J. P.; Primdal-Bengtson, B.; Dingli, F.; Loew, D.; Tkach, M.; Théry, C. Proteomic Comparison Defines Novel Markers to Characterize Heterogeneous Populations of Extracellular Vesicle Subtypes. *Proc. Natl. Acad. Sci. U.S.A.* **2016**, *113*, E968−E977.
(29) Rolls, M. M.; Webster, P.; Balba, N. H.; Rose, J. K. Novel Infectious Particles Generated by Expression of the Vesicular Stomatitis Virus Glycoprotein from a Self-Replicating RNA. *Cell* **1994**, *79*, 497−506.
(30) Shafiee, F.; Aucoin, M. G.; Jahanian-Najafabadi, A. Targeted Diphtheria Toxin-Based Therapy: A Review Article. *Front. Microbiol.* **2019**, *10*, 2340.
(31) Van Ness, B. G.; Howard, J. B.; Bodley, J. W. ADP-Ribosylation of Elongation Factor 2 by Diphtheria Toxin. Isolation and Properties of the Novel Ribosyl-Amino Acid and Its Hydrolysis Products. *J. Biol. Chem.* **1980**, *255*, 10717−10720.
(32) Yamaizumi, M.; Mekada, E.; Uchida, T.; Okada, Y. One Molecule of Diphtheria Toxin Fragment A Introduced into a Cell Can Kill the Cell. *Cell* **1978**, *15*, 245−250.
(33) Lange, M. J.; Lyddon, T. D.; Johnson, M. C. Diphtheria Toxin A-Resistant Cell Lines Enable Robust Production and Evaluation of DTA-Encoding Lentiviruses. *Sci. Rep.* **2019**, *9*, No. 8985.
(34) Mastrobattista, E.; Crommelin, D. J. A.; Wilschut, J.; Storm, G. Targeted Liposomes for Delivery of Protein-Based Drugs into the Cytoplasm of Tumor Cells. *J. Liposome Res.* **2002**, *12*, 57−65.
(35) Dancourt, J.; Piovesana, E.; Lavieu, G. Efficient Cell Death Mediated by Bioengineered Killer Extracellular Vesicles. *Sci. Rep.* **2023**, *13*, No. 1086.
(36) Picco, G.; Petti, C.; Trusolino, L.; Bertotti, A.; Medico, E. A Diphtheria Toxin Resistance Marker for in Vitro and in Vivo Selection of Stably Transduced Human Cells. *Sci. Rep.* **2015**, *5*, No. 14721.
(37) Corish, P.; Tyler-Smith, C. Attenuation of Green Fluorescent Protein Half-Life in Mammalian Cells. *Protein Eng. Des. Sel.* **1999**, *12*, 1035−1040.
(38) Metzelaar, M. J.; Wijngaard, P. L.; Peters, P. J.; Sixma, J. J.; Nieuwenhuis, H. K.; Clevers, H. C. CD63 Antigen. A Novel Lysosomal Membrane Glycoprotein, Cloned by a Screening Procedure for Intracellular Antigens in Eukaryotic Cells. *J. Biol. Chem.* **1991**, *266*, 3239−3245.
(39) Amara, J. F.; Clackson, T.; Rivera, V. M.; Guo, T.; Keenan, T.; Natesan, S.; Pollock, R.; Yang, W.; Courage, N. L.; Holt, D. A.; Gilman, M. A Versatile Synthetic Dimerizer for the Regulation of Protein-Protein Interactions. *Proc. Natl. Acad. Sci. U.S.A.* **1997**, *94*, 10618−10623.
(40) Uhlén, M.; Fagerberg, L.; Hallström, B. M.; Lindskog, C.; Oksvold, P.; Mardinoglu, A.; Sivertsson, Å.; Kampf, C.; Sjöstedt, E.; Asplund, A.; Olsson, I.; Edlund, K.; Lundberg, E.; Navani, S.; Szigyarto, C. A.-K.; Odeberg, J.; Djureinovic, D.; Takanen, J. O.; Hober, S.; Alm, T.; Edqvist, P.-H.; Berling, H.; Tegel, H.; Mulder, J.; Rockberg, J.; Nilsson, P.; Schwenk, J. M.; Hamsten, M.; von Feilitzen, K.; Forsberg, M.; Persson, L.; Johansson, F.; Zwahlen, M.; von Heijne, G.; Nielsen, J.; Pontén, F. Proteomics. Tissue-Based Map of the Human Proteome. *Science* **2015**, *347*, No. 1260419.
(41) Segel, M.; Lash, B.; Song, J.; Ladha, A.; Liu, C. C.; Jin, X.; Mekhedov, S. L.; Macrae, R. K.; Koonin, E. V.; Zhang, F. Mammalian Retrovirus-like Protein PEG10 Packages Its Own MRNA and Can Be Pseudotyped for MRNA Delivery. *Science* **2021**, *373*, 882−889.
(42) Blaise, S.; de Parseval, N.; Bénit, L.; Heidmann, T. Genomewide Screening for Fusogenic Human Endogenous Retrovirus Envelopes Identifies Syncytin 2, a Gene Conserved on Primate Evolution. *Proc. Natl. Acad. Sci. U.S.A.* **2003**, *100*, 13013−13018.
(43) Piccirillo, A. R.; Hyzny, E. J.; Beppu, L. Y.; Menk, A. V.; Wallace, C. T.; Hawse, W. F.; Buechel, H. M.; Wong, B. H.; Foo, J. C.; Cazenave-Gassiot, A.; Wenk, M. R.; Delgoffe, G. M.; Watkins, S. C.; Silver, D. L.; D'Cruz, L. M. The Lysophosphatidylcholine Transporter MFSD2A Is Essential for CD8+ Memory T Cell Maintenance and Secondary Response to Infection. *J. Immunol.* **2019**, *203*, 117−126.
(44) Ben-Zvi, A.; Lacoste, B.; Kur, E.; Andreone, B. J.; Mayshar, Y.; Yan, H.; Gu, C. Mfsd2a Is Critical for the Formation and Function of the Blood-Brain Barrier. *Nature* **2014**, *509*, 507−511.
(45) Lavieu, G.; Orci, L.; Shi, L.; Geiling, M.; Ravazzola, M.; Wieland, F.; Cosson, P.; Rothman, J. E. Induction of Cortical Endoplasmic Reticulum by Dimerization of a Coatomer-Binding Peptide Anchored to Endoplasmic Reticulum Membranes. *Proc. Natl. Acad. Sci. U.S.A.* **2010**, *107*, 6876−6881.
(46) Temoche-Diaz, M. M.; Shurtleff, M. J.; Schekman, R. Buoyant Density Fractionation of Small Extracellular Vesicle Sub-Populations Derived from Mammalian Cells. *Bio-Protocol* **2020**, *10*, No. e3706.

https://doi.org/10.1021/acsabm.2c00955
ACS Appl. Bio Mater. 2023, 6, 1081−1091